University of Glasgow
DEPARTMENT OF
AEROSPACE
ENGINEERING

Hot-Wire Measurements of Transverse Vortices

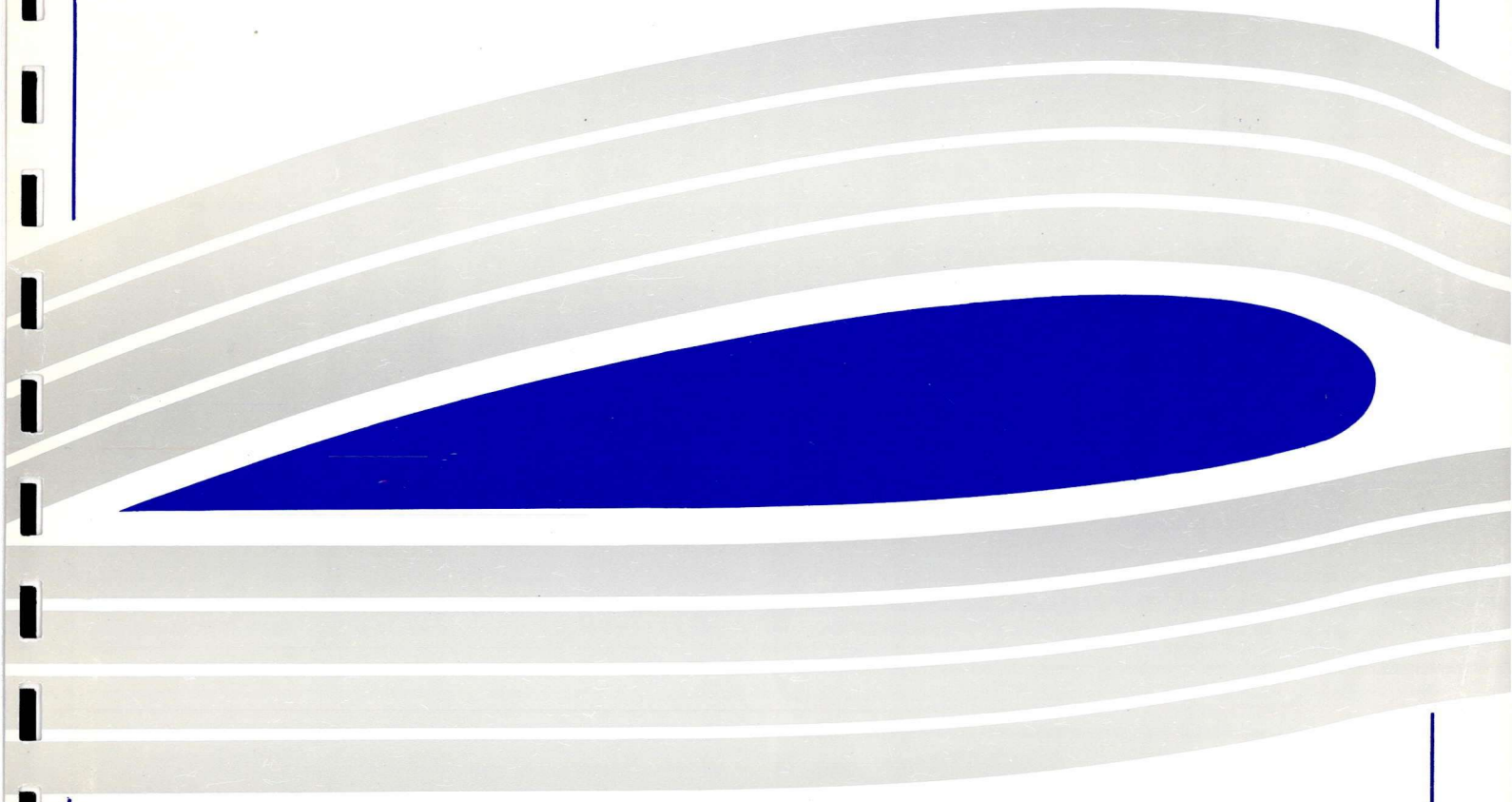

Hot-Wire Measurements of Transverse Vortices

Con Doolan
Department of Aerospace Engineering
University of Glasgow
Glasgow, Scotland, G20 8QQ

Glasgow University
Aerospace Engineering Report 9830

November, 1998

Technical Report 9830 B

Abstract

This is a report to document a series of tests performed using the new transverse vortex generator rig in the 1.15 m x 0.85 m wind tunnel. Results were acquired with a hot wire anemometer system using single and cross wire probes. A strong vortex velocity field was measured which confirmed the success of the vortex generation technique and provided information about the gross features of the flow. The data indicated that an interaction occured between the vortex core and the hot wire probe. This interaction manifested itself as variations in vortex core measurements which one would not expect without probe interference. While an interaction was present when measuring close to the core region, outside the core region the probe had little effect on vortex dynamics. This allowed analysis of vortex geometry and an estimation of the vortex wandering amplitude in the test section. Mechanisms of vortex/probe interaction were also considered and are discussed in the report. Wake curvature was measured using differently spaced single and cross wire probes. This data was compared with a computational model of the vortex generator wake and shows good agreement.

Nomenclature

c = rotor blade chord, m
d = vertical velocity peak-to-peak distance, m
k = constant for tip vortex strength (Stepniewski & Keys, 1984)
L_{TOT} = Total Blade Lift, N
r = vortex radius
u = measured freesteam velocity component, ms^{-1}
V = velocity, ms^{-1}
v = measured vertical velocity component, ms^{-1}
W = axial velocity, ms^{-1}
w = measured cross-stream velocity component, ms^{-1}
x = lateral distance from rotor shaft, distance from probe to vortex core, m
y = distance along tunnel centre line from rotor shaft, m
z = vertical from rotor shaft, m
Γ = circulation, m^2s^{-1}
Ω = rotation velocity of rotor, RPM or $rads^{-1}$
π = 3.14159...
ρ = density, kgm^{-3}

Subscripts and Superscripts

1 = vortex centre height
c = core radius
inf = freestream
p = peak
t = tip
vert = vertical component
θ = tangential
∞ = freestream

1 Introduction

Interactional aerodynamics has been identified as a cause of unwanted rotorcraft noise and vibration (Sheridan & Smith, 1980). Of particular concern is the three-dimensional vortex interaction, which typically involves a helicopter main rotor trailing vortex interacting with the tail section or fuselage. Understanding of the fluid dynamics of this event is essential in order to increase the performance and acceptance of future rotorcraft.

A number of practical acoustic studies concerning the helicopter tail rotor interaction can be found in the literature. Examples of these include in-flight and wind tunnel acoustics measurements (Samokhin, 1995; Schultz & Splettstoesser, 1993) and numerical studies (Howe, 1989; George & Chou, 1987). Other researchers found that noise levels could be lowered by a reducing of the tail rotor tip velocity (Jacobs *et al.*, 1997) or reversal of rotation direction (Leverton *et al.*, 1977) or both (Leverton & Pike, 1993). An in-flight study by Ellin (1993) considered the degradation in control produced by the tail rotor vortex interaction. These studies highlight the importance of the tail rotor vortex interaction for helicopter operation and design, however they leave the specific fluid dynamic mechanisms and structural response unresolved.

Concentrating on the interactional fluid dynamics, some experimental studies investigate the interaction of a rotor tip vortex and a large cylinder, representative of the helicopter fuselage (Liou *et al.*, 1990; Affes *et al.*, 1993; Affes *et al.*, 1998). Well resolved transient pressure and force coefficient data of the vortex tail boom interaction was obtained by Bi *et al.* (1993). Others studies involve the interaction of a blade or foil with a three-dimensional (3D) vortex, representing tail rotor BVI. Ahmadi (1986) measured radiated noise and limited surface pressure data from a blade chopping a fixed wing trailing vortex. High speed photography of this event is supplied by Cary (1987). More recently, flow visualization experiments have been performed by Marshall and Krishnamoorthy (1997; 1998) in support of a computational model of the normal vortex interation. Qualitatively, these studies show that once the 3D vortex has been cut or 'chopped' by the solid surface, the vortex core size increases or 'bulges' on one side and decreases or 'thins' on the other. The behaviour of the vortex core is controlled by the direction of the vortex core axial flow. On the side where the axial flow is directed toward the surface, the vortex bulges and conversely, on the side where the vortex thins, the axial flow is directed away from the surface (see Fig. 1). The vortex axial flow is a feature of rotor tip vortices which has been observed by other researchers (for example Conlisk (1998)) and is dependent on the loading and geometry of the rotor blade.

It can be observed that there is a lack of quality aerodynamic data for the 3D vortex interation with a blade in the available literature. Specifically, blade pressure and force coefficients of reasonable resolution are not yet available, especially for a main rotor/tail rotor configuration in foward flight. One of the problems in studying this phenomenon is the generation of a vortex in the laboratory. Efforts have been made in the past using a periodically pitching aerofoil (Booth & Yu, 1986), however this technique produces a twin, self-influencing vortex pattern without an axial core

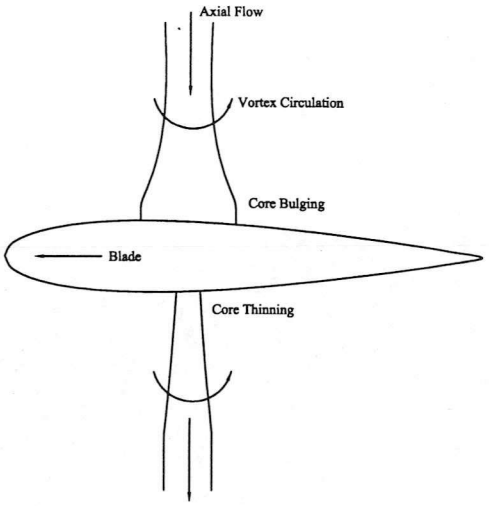

Figure 1: Illustration of vortex dynamics during vortex cutting.

flow which is not representive of a trailing tip vortex. In this work a new technique for generating a transverse, three-dimensional vortex is used. The method employs a rotor rig placed in the contraction of a wind tunnel which pitches a symmetrical blade through a simple profile as it rotates to generate a transverse vortex. This rig will be used in the future to study the interaction of a tansverse, 3D vortex with a blade. In the present work however, velocity measurements of the 3D vortex produced by this rig are presented.

2 Experimental Equipment

The experiments were conducted in the department's 1.15 m x 0.85 m low speed wind tunnel. This is a closed return facility capable of speeds up to 33 ms^{-1}. The test section length is 1.8 m in length. The free- stream conditions were monitored continuously using a pitot-static tube and thermocouple device.

The design of the transverse vortex generator is explained in detail by Copland (1997) and will be summarised here. The vortex generator consists of a single, variable pitch, rotating blade with a NACA 0015 cross section, positioned in the wind tunnel contraction. The blade has a rectangular planform of chord 0.1 m and tip radius 0.75 m from the hub centre. The blade pitch is varied using a spring loaded pitch link driven by a cylindrical cam. The cam profile is designed so that the blade pitch varies in four equivalent (90^o) phases of azimuth. The first phase sets the blade at zero incidence and occurs while the blade is pointing into the settling chamber (45^o azimuthal travel on either side of the wind tunnel centre line). In the next 90 degree phase, the blade is pitched from zero to 90^o. After this, the blade

passes the test section at constant 10^o incidence. In the final 90^o phase, the blade is returned to 0^o. In this region, the spring loaded link forces the blade to overcome its aerodynamic and inertial loads and follow the cam to return to zero degrees. A diagram outlining the operation of the vortex generator is shown in Figure 2.

The rotor rig is equipped with two optical sensors mounted on the rotating shaft. They are both of a simple and inexpensive design available from most electronics suppliers. The first sensor provides a measurement of the roational speed of the rig. The second is made available as an external trigger for a data acquisition device.

Velocity measurements were made using a TSI IFA-300 Hot Wire Anemometer system using DANTEC cross(X) wire probes. The cross wire probes used were 55P61 probes using 5 μm diameter platinum plated tungsten wires with a length-to-diameter ratio of 250. The measuring volume of the probe was approximately 0.8 mm in diameter and 0.5 mm in height. The wires were orientated 45^o to the free-stream and were perpendicular to each other.

The probe was calibrated in the wind tunnel using a special jig made for the purpose. During calibration, the probe was rotated (in 6^o steps) $\pm 30^o$ in the plane of the sensor wires to determine yaw sensitivity. A look-up table method was not used in preference to the yaw sensitivity method as documented by Copland (1997). Data was recorded at 10 kHz in 2048 bin samples. At each measurement point seventy, 2048 bin samples were ensemble averaged about the vortex centre position.

The probe was mounted in an automated, two-component traverse, mounted in this case on the floor, 1600 mm or 16 rotor chord lengths downstream of the rotating axis. The traverse was actuated by stepper motors controlled by a PC using LABVIEW software. The probe was positioned $x = -225$ mm to the left (looking towards the settling chamber) of the tunnel centreline and traversed vertically through $\delta z = 100$ mm. In its present configuration, the traverse is capable of measuring from the tunnel centreline through to 160 mm below ($z = -160$ mm). However, the vortex was not noticible above $z = -60$ mm, hence measurements were taken over the 100 mm range to $z = -160$ mm.

The $x = -225$ mm position was chosen for two reasons. Firstly, the vortex strength (taken to be the maximum vertical velocity peak-to-peak measured signal) is a maximum on this side of the test section because the tip vortex was created at the point where the blade tip has a maximum resolved normal component of velocity passing over it. Secondly, at the more intuitive probe location of the tunnel centreline, the vortex measurement was obscured by the wake shed by the vortex generator hub and support shaft. Interpretation of the vortex signal would have been easier if measurements could have be made at the centreline, as no correction

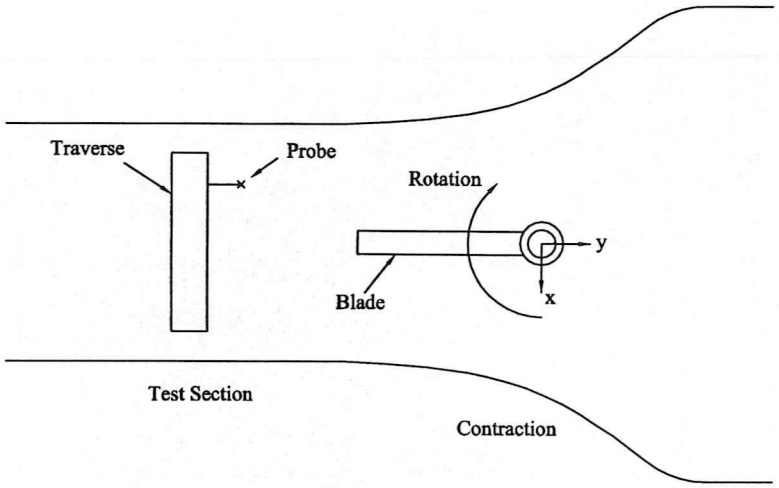

Plan View

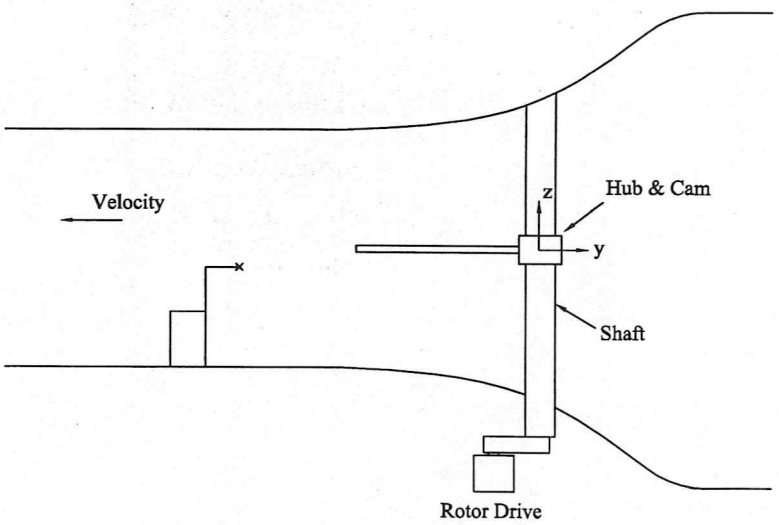

Side View

Figure 2: Diagram of transverse vortex generator.

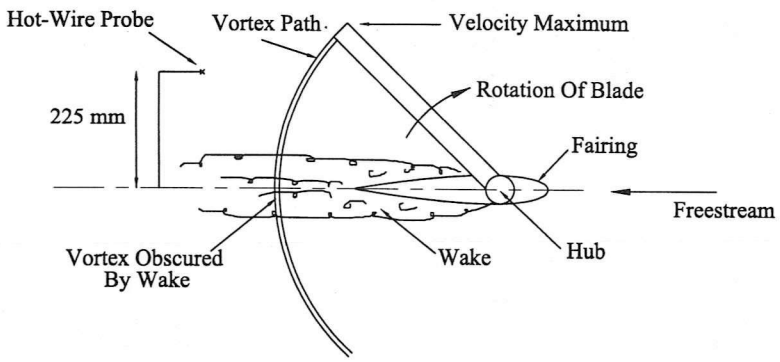

Figure 3: Choice of measurement position.

for vortex curvature would have been necessary. Figure 3 illustrates the reasons for the choice in measurement position.

After some initial variation of the various parameters (freestream velocity, rotor speed and probe position) operating parameters were set as freestream velocity, $V_\infty = 20$ ms^{-1} and rotational speed, $\Omega = 500$ RPM. This gave strong signals while maintaining acceptable aerodynamic loads on the rotor blade. No flapping hinge was provided in the rig so large bending moments occur at the root of the blade. These were kept below fatigue limits by operating at 500 RPM.

Tip vortex strength for a hovering rotor can be related to rotor thrust using the theory developed by Stepniewski and Keys (1984). A variation of this theory is presented here for the transverse vortex generator. Rotor thrust is calculated by discretizing the blade span and summing the lift produced at each blade element along the rotor blade for each azimuthal position. Non-dimensionialized tip vortex strength can then be calculated using,

$$\frac{\Gamma}{cR\Omega} = \frac{kL_{TOT}}{\rho cR^3\Omega^2} \tag{1}$$

where $k = 2$ (Stepniewski & Keys, 1984) and L_{TOT} is the lift produced on the blade at each azimuthal position.. Figure 4 shows the calculated variation of non-dimensionalized tip vortex strength with azimuth using Eq. 1 for the operating conditions outlined above. NACA 0015 aerofoil data was used to estimate lift. In this plot, 0^o indicates the start of the rotor phase where the blade is returned to zero incidence. Maximum non-dimensional operating parameters are displayed in Table 1.

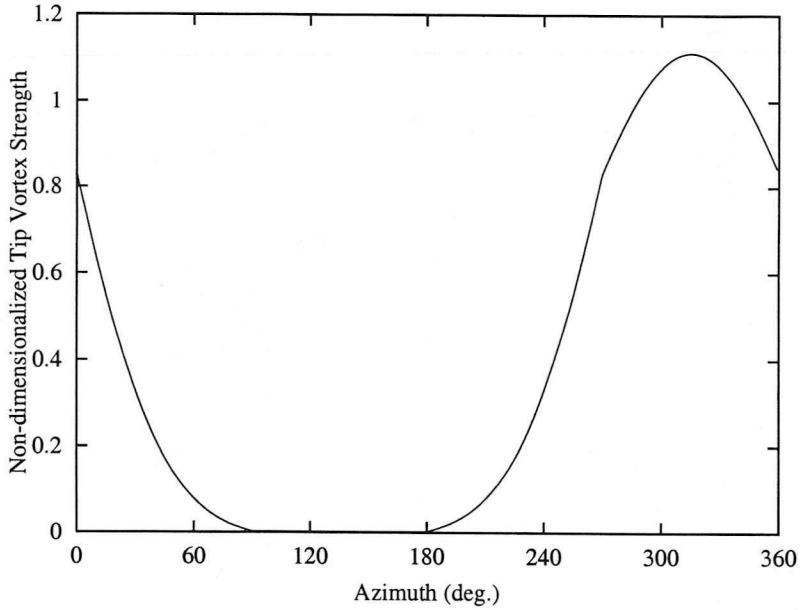

Figure 4: Variation of tip vortex strength with azimuth.

Table 1: Maximum blade tip non-dimensional operating parameters.

Tip Mach Number	0.18
Tip Reynolds Number	3.95×10^5
Tip Vortex Strength $(\frac{\Gamma}{cR\Omega})$	1.11
Tip Vortex Reynolds Number $(\frac{\Gamma}{\nu})$	3.0×10^5

3 Numerical Model

A numerical code was developed for the design of the vortex generator rig by Copland (1997). A full description of the code and its role in the design of the rig can be found in Copland (1997; 1995).

Briefly, the numerical model is based on a source panel representation of the wind tunnel walls. The rotor wake is modelled using a free wake vortex model consisting of a lattice of trailed and shed vortex elements generated by classical lifting line theory. This rotor wake is then convected though the wind tunnel using the local velocity which is determined by the source panel method.

This computational method is suited to the design of such a rig as it is able to model the accelerating effect of the wind tunnel contraction on the vortex system yet is computationally efficient. Hence operational parameters can be quickly varied to produce an optimal design.

In this section simulations of the vortex and wind tunnel flow experienced in the experiments are presented. The code parameters were set to, freestream velocity, $V_\infty = 20$ ms^{-1} and rotational speed, $\Omega = 500$ RPM.

Figure 5 shows the computed three-dimensional rotor wake structure as it convects through the contraction and test section. The wind tunnel air flow is in the negative y direction. The rotor shaft/centreline position is located at the origin and is represented by a dashed line and perpendicular rectangle. The contraction ends and the test section starts at $y = -1.30$ m. The model shows a well formed tip vortex is created and convected through the wind tunnel. A vortex sheet trails the tip vortex and extends below the tip vortex centreline.

Figure 6 shows the trajectory of the tip vortex as it travels through the wind tunnel. The slope of the trajectories are reasonably straight indicating a constant speed through the wind tunnel, equal to the freestream velocity. The separation of the two vortex paths is identical to the inverted rotor frequency, 8.33 Hz. This result was confirmed during experiment. Hence, successive tip vorticies are separated by 24 chord lengths and have little influence on each other as they convect through the wind tunnel. Measurement of the vortex angle (θ) (see Figure 7) shows the vortex passes the measurement location at 41.2^o.

4 Experimental Results

Interpretation of the hot wire vortex information is complicated by the inclination of the vortex with respect to the probe. In a three-dimensional vortex, the cross wire

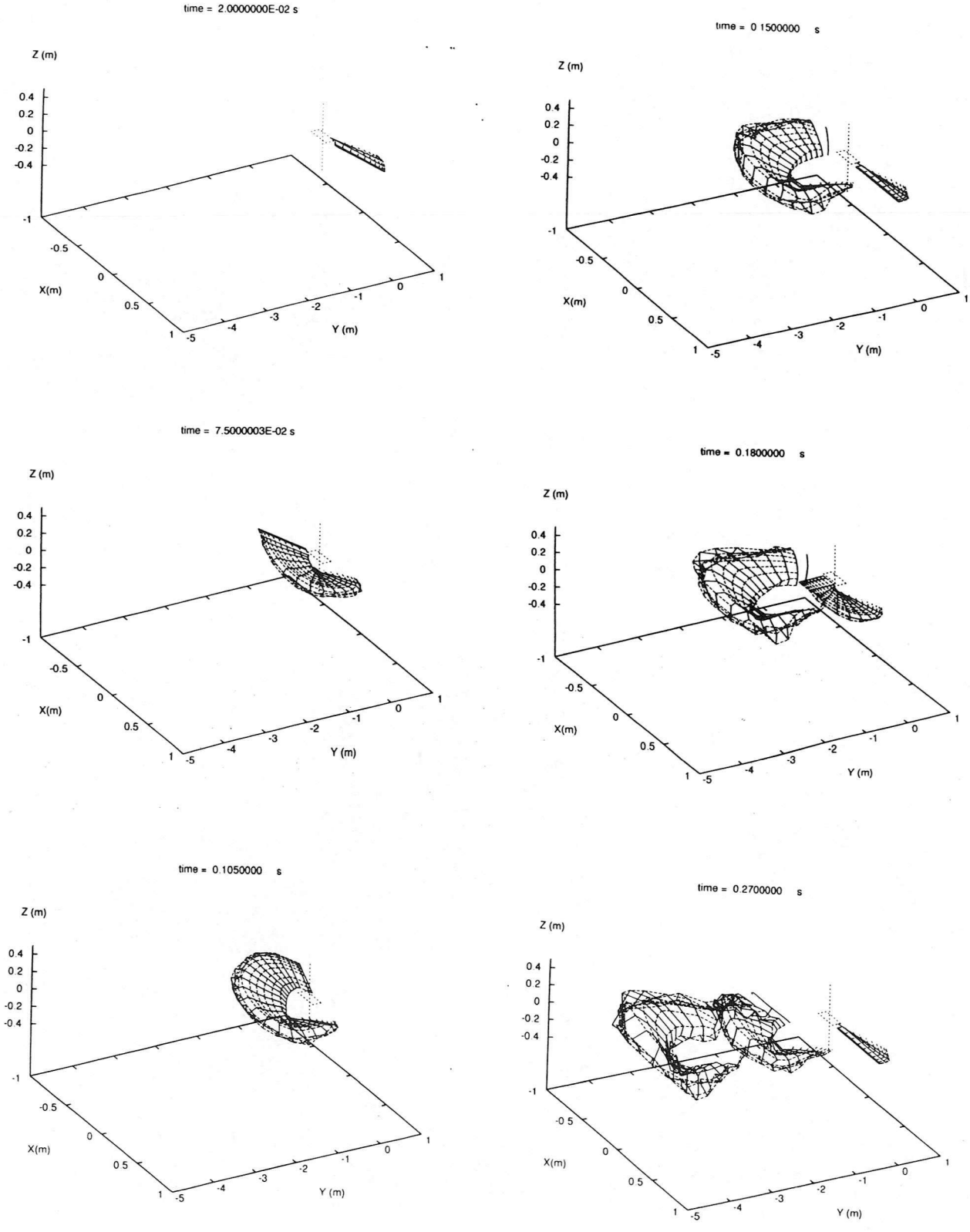

Figure 5: Wake structure as it convects through wind tunnel.

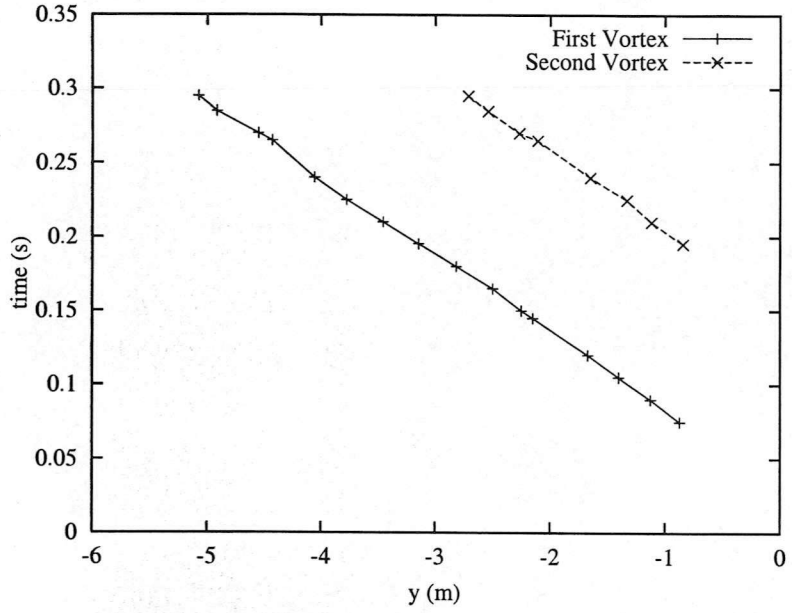

Figure 6: Trajectory of tip vortex.

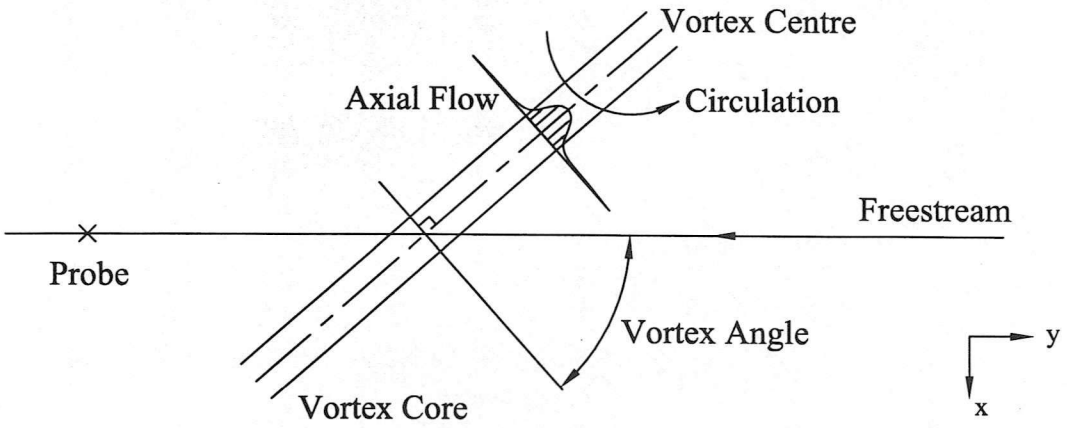

Figure 7: Plan view of convecting vortex segment - definition of vortex angle.

probe will measure a combination of vortex velocity components (i.e. tangential and axial), as illustrated by Figure 7.

Interpretation is further complicated by vortex wandering. Each successive vortex does not follow the same path as it travels through the test section. For analysis, this corresponds to a different core centre vertical distance with respect to the probe for each vortex passage. The consequences of wandering are that the vortex parameters measured by the probe can vary significantly for each vortex passage at the same z location. Ensemble averaging the vortex signals will therefore 'smear' or convolve the vortex reading to produce a result only indicative of the vortex produced. However, ensemble averaging is useful for obtaining geometry details of the vortex flow field.

Interaction with the cross wire probe also confuses matters. The conventional model of a free vortex consists of a viscous core surrounded by first a turbulent sheath and then by largely an inviscid external flow. It is argued here that while the probe interacts strongly with the vortex core region, the probe has little effect on vortex dynamics when measuring in the external field. Using this assumption, details of the tip vortex can be obtained by an ensemble averaged traverse through the flow field.

4.1 Raw Data

Figure 8 shows two typical measurements using the cross wire probe taken at $z = -119$ mm. In Fig. 8(a) the probe was orientated at 0^o, hence it measures the vertical and freestream component and in Figure 8(b) the probe was orientated at 90^o measuring cross flow and freestream components. The sense of the measurement is as illustrated by the coordinate axes in Fig. 2.

The measurements show a reasonably strong vortex signal was measured at the probe location. In the vertical component the vortex signal was superimposed on a constant downward momentum flux which was due to the action of the rotor on the flow. This momentum flux was removed for analysis by subtracting the time averaged vertical velocity from the data record.

Also, simultaneously occuring spikes or 'drop outs' are displyed on the raw data records. The origin of these anomalies are unknown but are thought to be due to inference between the variable frequency motor controller used to control rotor speed and the hot-wire system electronics. Attempts were made during testing to isolate the noise but were unsuccessful.

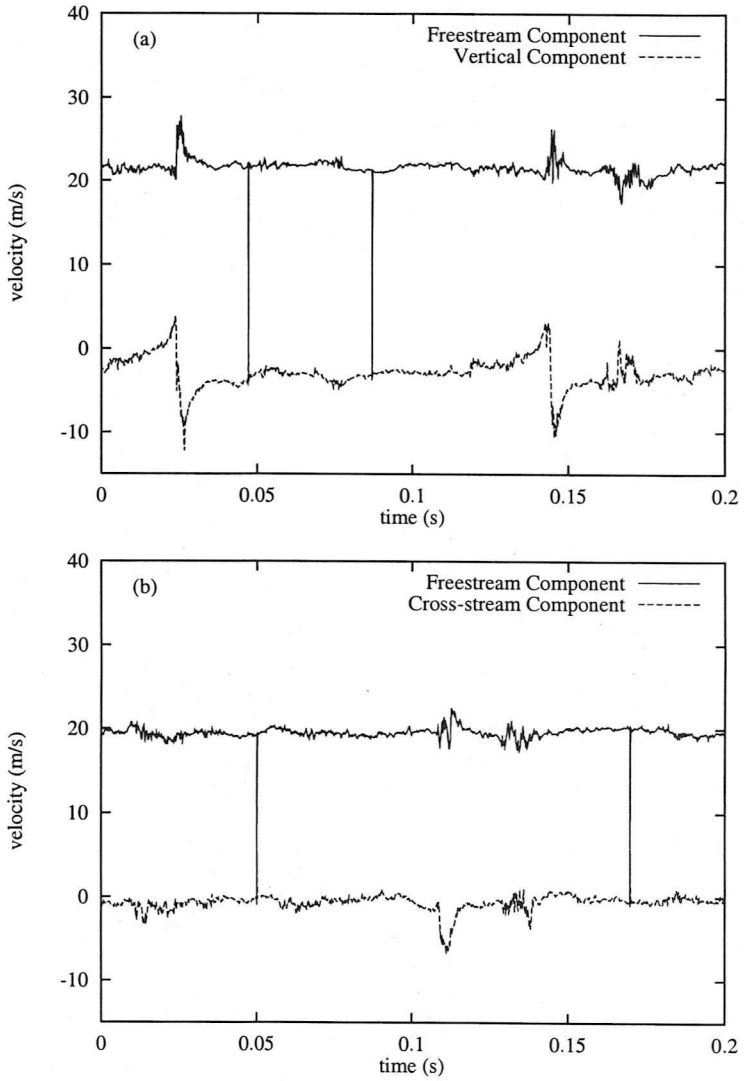

Figure 8: Raw data obtained from hot-wire system, (a) 0^o probe rotation, (b) 90^o rotation.

4.2 Ensemble Averaging

The probe was positioned at twenty vertical (z) locations over the 100 mm vertical range. At each position seventy, 2048 bin samples were ensemble averaged at each probe orientation to produce average time resolved records for the three components of velocity.

Figure 9 shows normalized ensemble averaged measurements of the vertical and cross-stream components of velocity at $z = -115$ mm. The time has been converted to a normalized distance using the time averaged freestream component and rotor chord length (x/c) where $x/c = 0$ indicates the centre of the vortex. This result is similar in form to other measurements in the traverse range. The vertical velocity is a resolved component of the tangential vortex velocity if the tilt of the vortex in the xy plane is not large. The peak-to-peak distance, d between the vertical velocity peaks is a measure of the distance across the circle enclosed by a streamline of maximum tangential velocity[1] for a particular vertical distance or z_1 value. Figure 10 defines the d measurement. If vortex/probe interaction did not exist, the d measurement would be an accurate indicator of core size.

The vertical velocity data shows unequal velocity magnitudes on either side of the vortex centre. This can be explained by the fact that the vortex is curved, more or less in the shape of a half ring. The self influence of the vortex increases the velocity on the inner side or side closest to the rotor. This is a result observed in other rotor flows, for example (Han *et al.*, 1997).

Figure 9(b) shows the ensemble averaged cross-stream component and is considered a combination of axial and tangential velocities due to vortex curvature. The record shows a peak near the vortex centre. This can be compared with theory to increase understanding about the vortex produced.

4.3 Comparison to Theory

Results from the traverse can be compared to simple vortex theory to obtain increased understanding of the transverse vortex and the limitations of the hot-wire technique to measuring this vortex system.

A Lamb type vortex is assumed to be adequate in describing the flow generated by the rig. This has been found to work well for other rotor generated vortices (Han *et al.*, 1997). The mathematical form used here is,

$$V_\theta = \frac{\Gamma}{2\pi r}[1 - e^{-r^2/r_c^2}] \tag{2}$$

[1] Assumed in the absence of the freestream velocity.

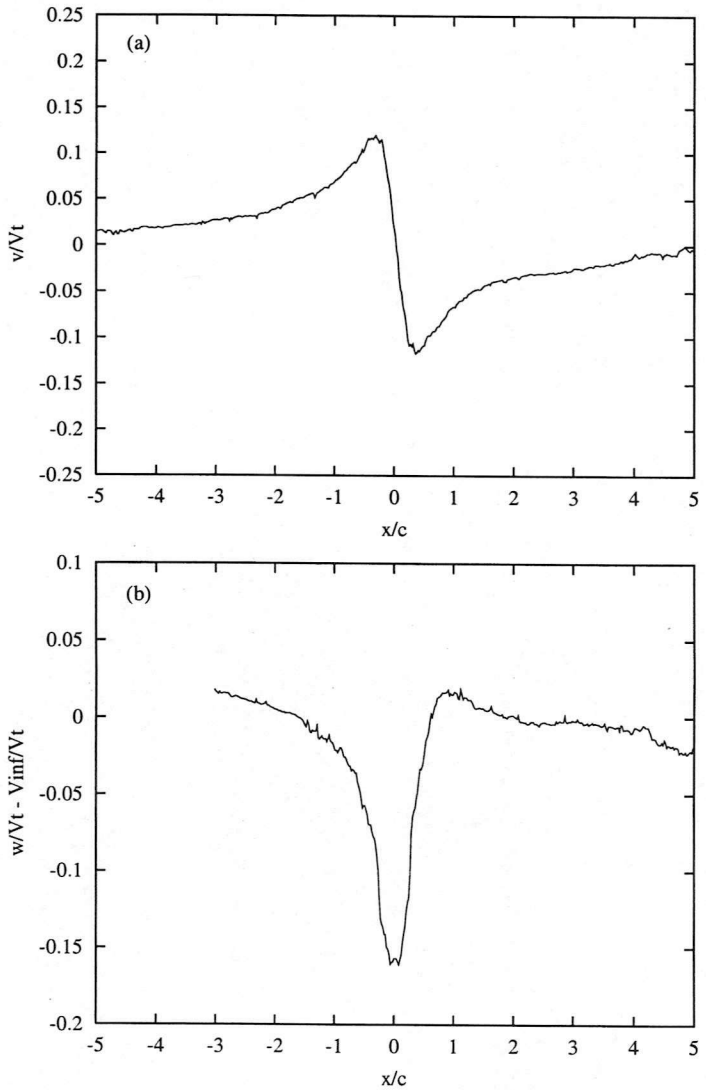

Figure 9: Normalized ensemble averaged hot-wire data, (a) Vertical component, (b) Cross stream component.

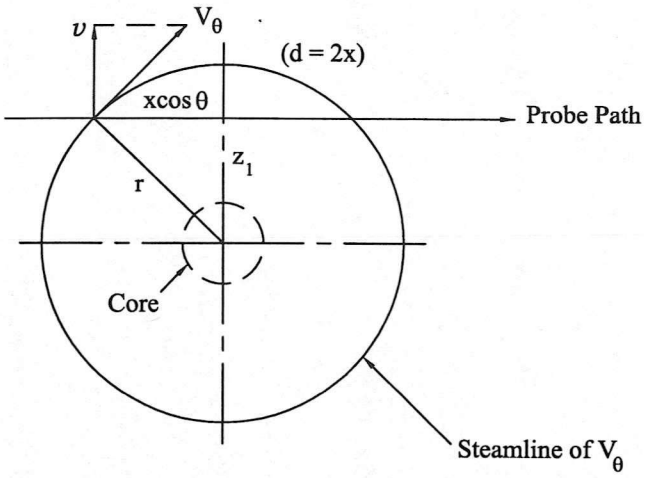

Figure 10: Sketch explaining the d measurement of the vortex flow.

$$W = W_m \, e^{-r^2/r_c^2} \tag{3}$$

The radial component is assumed negligible. The distance r from the vortex centreline is described by,

$$r^2 = x^2 \cos^2\theta + z_1^2 \tag{4}$$

where θ is the vortex angle, x is the stream wise distance from the vortex centreline and z_1 is the vertical displacement of the vortex centre above the probe.

The vertical component of tangential velocity is essentially what is measured by the hot-wire probe at 0^o rotation (v measurement). Therefore, the measurement d can be estimated from the vertical tangential component,

$$V_{\theta,vert} = \frac{\Gamma x \cos\theta}{2\pi r^2}[1 - e^{-r^2/r_c^2}] \tag{5}$$

The x value corresponding to maximum vertical velocity can be found by taking the derivative with respect to x and finding the root of the resulting equation, which reduces to,

$$0 = [1 - e^{-r^2/r_c^2}]\left[1 - \frac{2x^2\cos^2\theta}{r^2}\right] + \frac{2x^2\cos^2\theta}{r_c^2} e^{-r^2/r_c^2} \tag{6}$$

An estimate of the d measurement is twice the root (x) value obtained.

A simple numerical scheme was devised to solve for x for each z location set by the traverse position. By assuming a core size of 15% of the chord and using the estimate of vortex angle (curvature) obtained from the source panel numerical code, the roots of the equation were obtained and compared to the experimental results, Figure 11.

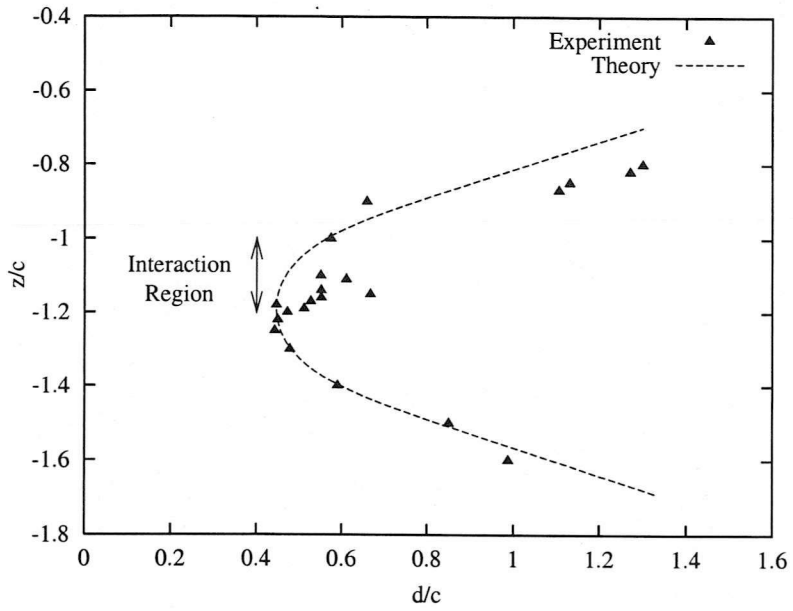

Figure 11: Comparison of d measurements with theory.

Reasonably good agreement between theory and experiment is found outside the 'core region' as marked on the figure. In the core region, there is little agreement, which suggests a strong interaction with the hot wire probe. The size of the interaction region is larger than the core size due to the action of vortex wandering.

This result indicates that outside the core region, the probe has little influence on vortex dynamics and the good agreement with the simple theory indicates that the numerical model predicts the vortex curvature well. Using this, an estimate of the vortex wandering can be made. Taking a point outside of the vortex interaction region (in this case $z = -150$ mm), equation 2 can be solved for z_1 for each individual measurement of $d/2$ at that traverse position. Seventy individual measurements were made at each z location. Taking the root-mean-square of the calculated z_1 values gives a mean wandering amplitude of 29.5 mm.

Further information can be obtained from the peak measurements in the cross flow component measurements. This maximum cross flow value is labelled Wp. Assuming the peak cross stream velocity occurs when the vortex passes the probe, the following can estimate its value through the traverse,

$$Wp = W\cos\theta - V_\theta \sin\theta \tag{7}$$

where V and W are functions of r and are given by equations 2 and 3 respectively.

Equation 7 gives a best fit to the data (Figure 12) by using the previous estimates of core size and θ and by assuming a circulation strength of $\Gamma = 0.65$ m^{2}s^{-1} and

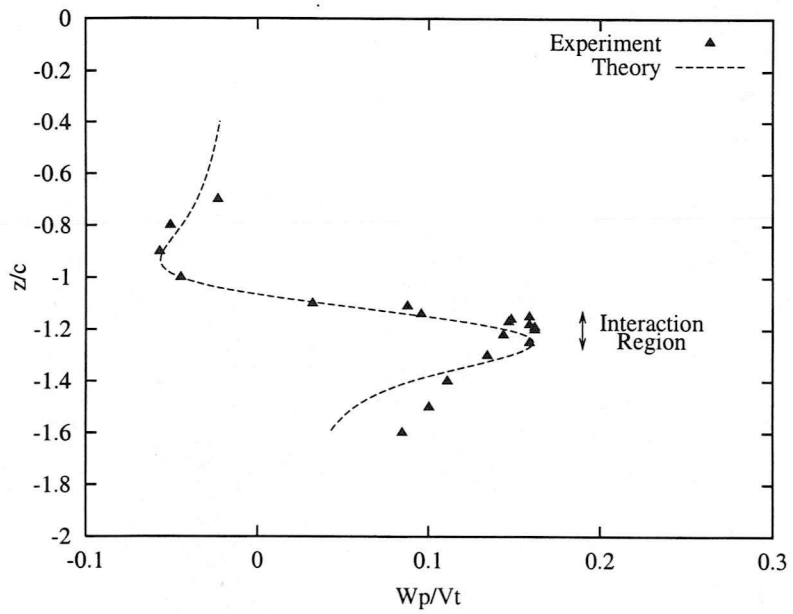

Figure 12: Comparison of Wp measurements with theory.

a maximum axial flow of $W_m = 7.25$ ms^{-1}. Again reasonable agreement is found outside the core region where the probe does not interfere with the vortex. The agreement is poor in the lower portion of the plot, this is thought to be due to vortex wandering. The assumed values used to obtain this agreement are notional only. They are tempered by the effects of vortex wandering and by the assumptions used in modelling the basic vortex structure. To obtain accurate core measurements, a non-intrusive technique will need to be implemented.

4.4 Geometry Measurement

In a separate test, simultaneous cross and single wire probe measurements were obtained with various lateral (δx) separation distances between them. Setting the vertical height of the probe outside of the interaction region, the measured time difference between the vortex passing each probe is a direct measurement of relative wake position. These measurements were compared with a two-dimensional projection of the computed wake structure at an equivalent time, which is shown in Fig. 13. Very good agreement is observed, which gives confidence to the $\theta = 41.2^o$ assumption used in the analytical theory. It also suggests the coupled panel method and free wake model provides an accurate representation of the wake geometry in the the wind tunnel.

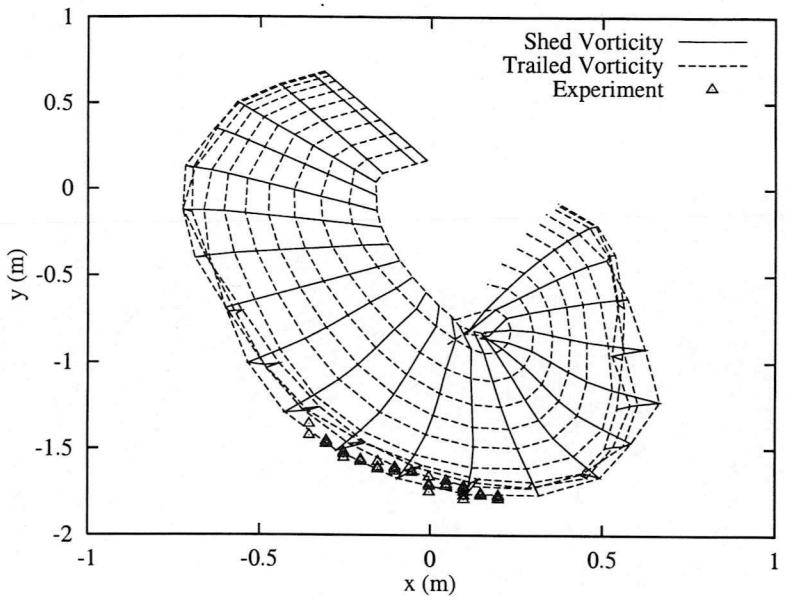

Figure 13: Comparision of computed wake geometry with experiment.

5 Vortex/Probe Interaction Mechanisms

The results obtained from hot wire measurements indicate that there is a fluid-structure interaction between the probe body and the vortex core. The exact mechanism of this interaction is unclear however, two mechanisms are proposed based on previously observed phenomena in the literature. These mechanisms could act either separately or in unison.

The first proposed mechanism is self induced vortex movement. This fluid structure mechanism is documented by Ziada and Rockwell (1982). In this work, two-dimensional vortices were created by a mixing layer instability and allowed to interact with a sharp leading edge. It was found that as the vortex approached the leading edge, it tended to 'dive' to the underside of the wedge due to the velocity field interaction with the surface. This was observed even when the vortex centre was initially above the leading edge. It is proposed that a similar mechanism may occur with the 3D vortex. This is partially supported by the results in Fig. 10 which shows an interaction region asymmetric about the mean vortex centre position.

The second mechanism is core penetration by the probe. As discussed earlier, the mechanism for complete vortex cutting by a blade involves 'bulging' and 'thinning' of the core, depending on the direction of axial flow. Analytical and computational models of this are well documented by Lundgren and Ashurst (1989), Marshall and Krishnamoorthy (1997) and Lee *et al.* (1998). For the present work it is proposed that within the core region the probe may penetrate the core, which would induce

an area-varying wave to travel along the vortex. The initiation of this wave should cause some change in the core radius. Again, this is supported by the experimental results in Fig. 10 which shows distinct core radius reduction in the interaction region.

These models are speculative only. To obtain an accurate model of the interaction mechanism a flow visualization technique needs to be implemented.

6 Conclusions and Future Work

This report documents hot-wire tip vortex measurements performed in the 1.15 m x 0.85 m wind tunnel with the new transverse vortex generator. Results show that the technique is capable of producing a well defined vortex, typical of a rotor in forward flight. More detailed measurements indicate that a strong interaction occurs between the core and the hot-wire probe however, little influence is noticed in the region external to the core. Using this information, gross features of the flowfield can be determined and compare well to the source panel numerical model. The vortex wandering amplitude was estimated to be 29.5 mm.

The interaction of the vortex with the probe requires the application of a non-intrusive measurement technique to accurately obtain information about the vortex structure. This represents the next stage of the project, with a particle image velocimetry system being installed in the 1.15 m x 0.85 m wind tunnel. An instrumented blade will be placed in the path of the vortex so non-intrusive measurements of the vortex during blade interaction can be made in conjunction with surface pressure data. The laser system will also be used for flow visualization studies of probe/vortex interaction.

At the time of writing, a large scale transverse vortex generator is under construction to be later installed in the 2.65 m x 2.04 m wind tunnel. This rig will provide a much stronger vortex flow field (blade tip Reynold's number of 2.5×10^6) and incorporates a rotor hub which includes a 5^o pre-cone and is supported entirely from below in contrast to the present rig. This will allow measurement of the vortex with zero vortex angle free from hub and support shaft wake interference.

Acknowledgements: This work was funded by the Engineering and Physical Sciences Reseach Council. The author would also like to thank C.Copland for the design of the vortex generator rig.

References

AFFES, H., CONLISK, A.T., KIM, J.M., & KOMERATH, N.M. 1993. Model for Rotor Tip Vortex-Airframe Interaction Part 2: Comparison with Experiment. *AIAA Journal*, **31**(12), 2274–2282.

AFFES, H., XIAO, Z., CONLISK, A.T., KIM, J.M., & KOMERATH, N.M. 1998. Model for Rotor Tip Vortex-Airframe Interaction Part 3: Viscous Flow on Airframe. *AIAA Journal*, **36**(3), 409–415.

AHMADI, A.R. 1986. An Experimental Investigation of Blade-Vortex Interaction at Normal Incidence. *AIAA Journal*, **23**(1), 47–55.

BI, N., LEISHMAN, J.G., & CROUSE, G.L. 1993. Investigation of Rotor Tip Vortex Interactions with a Body. *Journal of Aircraft*, **30**(6), 879–888.

BOOTH, E.R, & YU, J.C. 1986. *New Technique for Experimental Generation of Two-Dimensional Blade-Vortex Interaction at Low Reynolds Number.* Tech. rept. NASA TP-2551. NASA.

CARY, C.M. 1987 (September). *An Experimental Investigation of the Chopping of Helicopter Main Rotor Tip Vorticies by the Tail Rotor. Part II: High Speed Photographic Study.* Contractor Report 177457. NASA.

CONLISK, A.T. 1998 (June). A Theory of Vortex-Surface Collisions. *In: AIAA Paper No: 98-2858.*

COPLAND, C.M. 1997. *Methods of Generating Vortices in Wind Tunnels.* Ph.D. Thesis. Department of Aerospace Engineering, University of Glasgow.

COPLAND, C.M., COTON, F.N., & GALBRAITH, R.A.McD. 1995. *Use of a numerical model in the conceptual design of a new blade vortex interaction facility.* Research Report No. 9509. University of Glasgow.

ELLIN, A.D.S. 1993 (Sept.). An In-Flight Investigation of Lynx AH Mk5 Main rotor/Tail Rotor Interactions. *In: 19th European Helicopter Forum.*

GEORGE, A.R., & CHOU, S.T. 1987 (March). *Helicopter Tail Rotor Blade-Vortex Interaction Noise.* Contractor Report 183178. NASA.

HAN, Y.O., LEISHMAN, J.G., & COYNE, A.J. 1997. Measurements of the Velocity and Turbulence Structure of a Rotor Tip Vortex. *AIAA Journal*, **35**(3), 477–485.

HOWE, M.S. 1989. On Unsteady Surface Forces, and Sound Produced by the Normal Chopping of a Rectilinear Vortex. *Journal of Fluid Mechanics*, **206**, 131–153.

JACOBS, E.W., MANCINI, J., VISINTAINER, J.A., & JACKSON, T.A. 1997. Acoustic Flight Test Results for the Sikorsky S-76 Quiet Tail Rotor at Reduced Tip Speed. *In: American Helicopter Society 53rd Annual Forum.* Viginia Beach, Virginia: AHS.

KRISHNAMOORTHY, S., & MARSHALL, J.S. 1998. Three-Dimensional Blade Vortex Interaction in the Strong Vortex Regime. *Submitted to Physics of Fluids.*

LEE, J.A., BURGGRAF, O.R., & CONLISK, A.T. 1998. On the Impulsive Blocking of a Vortex Jet. *Journal of Fluid Mechanics*, **369**, 301–331.

LEVERTON, J.W., & PIKE, T.C. 1993. The Importance of Tail Rotor Interaction as an Acoustic Source. *In: American Helicopter Society 49th Annual Forum.* St Louis, Missouri: AHS.

LEVERTON, J.W., POLLARD, J.S., & WILLS, C.R. 1977. Main Rotor Wake/Tail Rotor Interaction. *Vertica*, **1**, 213–221.

LIOU, S.G., KOMERATH, N.M., & MCMAHON, H.M. 1990. Measurement of the Interaction Between a Rotor Tip Vortex and a Cylinder. *AIAA Journal*, **28**(6), 975–981.

LUNDGREN, T.S., & ASHURST, W.T. 1989. Area-varying Waves on Curved Vortex Tubes with Application to Vortex Breakdown. *Journal of Fluid Mechanics*, **200**, 283–307.

MARSHALL, J.S., & KRISHNAMOORTHY, S. 1997. On the Instantaneous Cutting of a Columnar Vortex with Non-Zero Axial Flow. *Journal of Fluid Mechanics*, **351**, 41–74.

SAMOKHIN, V.F. 1995 (Aug.30 - Sept.1). Impulsive Noise of the Helicopter Tail Rotor. *In: 21st European Helicopter Forum.*

SCHULTZ, K.J., & SPLETTSTOESSER, W.R. 1993. Helicopter Main Rotor/Tail Rotor Noise Radiation Characteristics from Scaled Model Rotor Experiments in the DNW. *In: American Helicopter Society 49th Annual Forum.* St Louis, Missouri: AHS.

SHERIDAN, P.F., & SMITH, R.P. 1980. Interactional Aerodynamics - A New Challenge to Helicopter Technology. *Journal of American Helicopter Society*, **25**, 3–21.

STEPNIEWSKI, W.Z., & KEYS, C.N. 1984. *Rotary-Wing Aerodynamics.* New York: Dover Publications.

ZIADA, S., & ROCKWELL, D. 1982. Vortex-Leading-Edge Interaction. *Journal of Fluid Mechanics*, **118**, 79–107.